Nanofiber Yarn/Hydrogel Core–Shell Scaffolds Mimicking Native Skeletal Muscle Tissue for Guiding 3D Myoblast Alignment, Elongation, and Differentiation

Ling Wang,[†,¶] Yaobin Wu,[†,¶] Baolin Guo,[*,†] and Peter X. Ma[*,†,‡,§,∥,⊥]

[†]Center for Biomedical Engineering and Regenerative Medicine, Frontier Institute of Science and Technology, Xi'an Jiaotong University, Xi'an 710049, China and [‡]Department of Biomedical Engineering, [§]Department of Biologic and Materials Sciences, [∥]Macromolecular Science and Engineering Center, and [⊥]Department of Materials Science and Engineering, University of Michigan, Ann Arbor, Michigan 48109, United States. [¶]L.W. and Y.W. contributed equally to this work.

ABSTRACT Designing scaffolds that can mimic native skeletal muscle tissue and induce 3D cellular alignment and elongated myotube formation remains an ongoing challenge for skeletal muscle tissue engineering. Herein, we present a simple technique to generate core–shell composite scaffolds for mimicking native skeletal muscle structure, which comprise the aligned nanofiber yarn (NFY) core and the photocurable hydrogel shell. The aligned NFYs are prepared by the hybrid composition including poly(caprolactone), silk fibroin, and polyaniline *via* a developed dry–wet electrospinning method. A series of core–shell column and sheet composite scaffolds are ultimately obtained by encapsulating a piece and layers of aligned NFY cores within the hydrogel shell after photo-cross-linking. C2C12 myoblasts are seeded within the core–shell scaffolds, and the good biocompatibility of these scaffolds and their ability to induce 3D cellular alignment and elongation are successfully demonstrated. Furthermore, the 3D elongated myotube formation within core–shell scaffolds is also performed after long-term cultivation. These data suggest that these core–shell scaffolds combine the aligned NFY core that guides the myoblast alignment and differentiation and the hydrogel shell that provides a suitable 3D environment for nutrition exchange and mechanical protection to perform a great practical application for skeletal muscle regeneration.

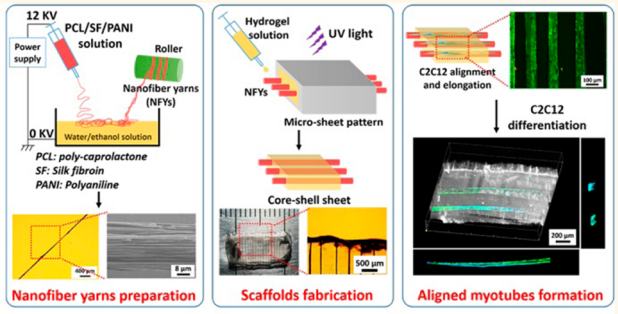

KEYWORDS: nanofiber yarns · core–shell scaffold · 3D cellular alignment · myogenic differentiation · skeletal muscle regeneration

Skeletal muscles are the tissues in the human body that are mainly responsible for generating force and facilitating voluntary movement. In general, skeletal muscles have an endogenous ability to regenerate through the activation of resident satellite cells.[1,2] However, under compromised conditions, severe trauma would cause the loss of muscle functionality and these injuries are irreversible.[3] Recently, tissue engineering strategies have demonstrated potential applications for skeletal muscle regeneration, and a tissue engineering scaffold represents a key tool to control and guide tissue regeneration.[4−9] Skeletal muscle is a highly organized tissue comprising aligned myofibers formed through myoblasts fused together into multinucleated myotubes surrounded within an extracellular connective tissue (Figure 1a).[8,10,11] The specific alignment of myofibers is essential for force generation, and furthermore, the connective tissue can maintain muscle shape and allow the myofibers to contract in synergy during movement.[12] Therefore, to effectively mimic the native structure and replicate the biological function of skeletal muscle tissue, developing tissue engineering scaffolds that can control cellular organization and alignment within a three-dimensional (3D) environment would be highly beneficial for skeletal muscle regeneration.

Recently, there have been significant efforts in controlling 2D cellular organization

* Address correspondence to baoling@mail.xjtu.edu.cn, mapx@umich.edu.

Received for review June 16, 2015 and accepted August 17, 2015.

Published online August 17, 2015
10.1021/acsnano.5b03644

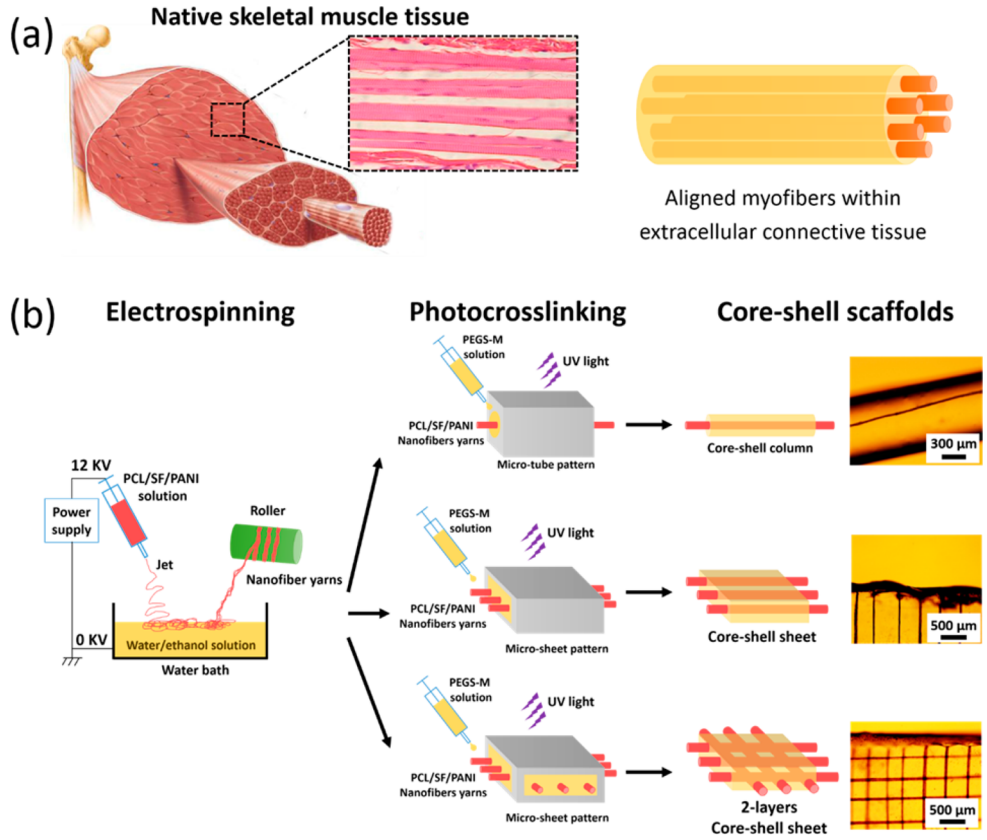

Figure 1. (a) Composite resembles the structure of skeletal muscle tissue, consisting of aligned myofibers formed through myoblast fusion together into multinucleated myotubes surrounded within the extracellular connective tissue. (b) Preparation scheme of core–shell column and sheet scaffolds that mimic the native skeletal muscle tissue by the combination of aligned nanofiber yarns *via* electrospinning and hydrogel shell *via* photocurable microfabrication of poly(ethylene glycol)-*co*-poly(glycerol sebacate) (PEGS-M) solution.

and alignment in defined microarchitectures such as fibers, grooves, and pits created by chemical or topographic patterning.[13−19] Among these techniques, electrospinning aligned fibers have been widely used in skeletal muscle tissue engineering because they can mimic the anisotropic structural organization of native skeletal muscle and their nano- and microstructures can provide guidance cues to direct aligned myotube formation.[20−23] Nonetheless, in most cases, cells seeded on the electrospinning nanofiber scaffolds are unable to infiltrate into the mesh due to the dense nanofiber structure and the limited thickness, which are limited to guiding cellular alignment in 2D. Designing a scaffold that can guide the aligned and elongated myotube formation within a 3D environment is still a challenge.

In some studies, aligned myotube formation within 3D scaffolds has been induced by incorporating elongated pores into the 3D scaffolds by using freeze-drying and phase separation methods.[24−26] However, uniform cell seeding and distribution inside these 3D scaffolds are difficult due to the low interconnectivities between elongated pores in the scaffolds. In contrast, cells can be easily encapsulated and then cultured within hydrogel scaffolds homogeneously, which shows a similar 3D environment with native tissues.[27−29] Furthermore, some research shows that myoblasts embedding in collagen hydrogels performed 3D cellular alignment and elongated myotube formation under mechanical stimulation, but unfortunately, the inconvenience of controlling the external cell stimuli still limits their possible applications.[30−32] Although there are some simple approaches to recreate the 3D cellular alignment architectures within micropatterning hydrogels without the need for external stimulation, the thickness limitation of these micropatterning hydrogels is a large barrier for their practical use.[33−35] In addition, by incorporating nanofibers within the hydrogel, the composite scaffolds with dimensions ranging from micro- to macroscale have been fabricated to improve cell adhesion and proliferation within the 3D environment and to also enhance the scaffolds' mechanical properties.[36−39] However, there are few studies about developing a scaffold that can mimic the native skeletal muscle tissue and can induce 3D cellular alignment and elongated myofiber formation without external stimulation.

In this work, we present core–shell composite scaffolds comprising the aligned nanofiber yarn (NFY) core that mimic the myofibers' aligned structure and

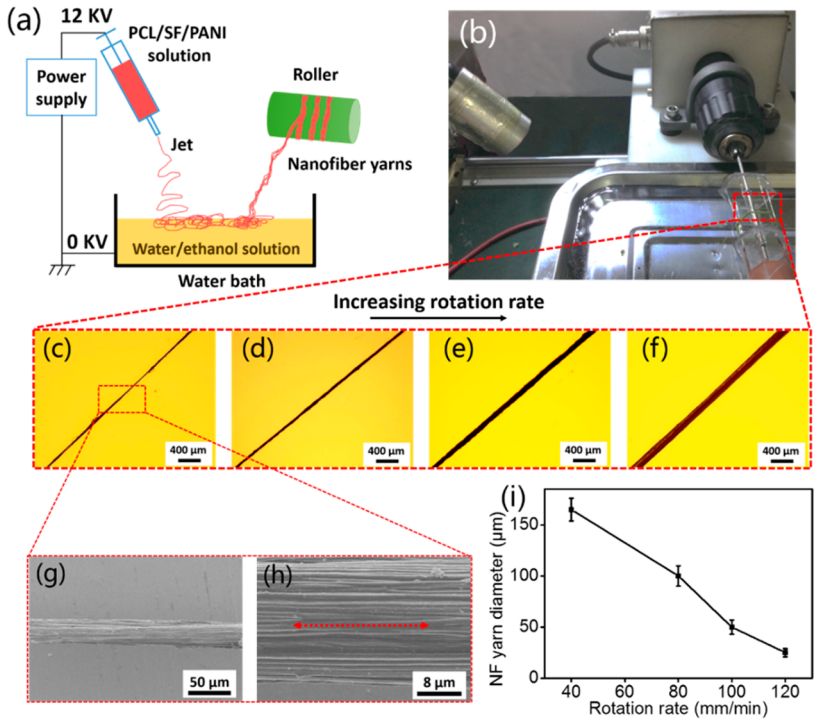

Figure 2. Fabrication of PCL/SF/PANI aligned nanofiber yarns by a developed dry–wet electrospinning method. (a) Scheme of the experimental setup composed of a series of electrospinning devices, a water bath containing water/ethanol solution, and a rotating receptor. The nanofiber web is formed on the liquid surface when the PCL/SF/PANI solution is jetted out of the syringe in the presence of a high voltage, and then this nanofiber web is drawn and lifted off the liquid surface by a rotating receptor to form continuously aligned NFYs. (b) Actual fabricated devices are in use. (c–f) Aligned NFYs are collected with the rotating receptor at different rotation speed. Scale bars = 400 μm. (g) Microstructure of aligned NFYs is observed by SEM, and the higher magnification image shows continuous nanofibers organized with the same orientation (h). (i) Variation of aligned NFY diameter as a function of rotation speed. Error bars are standard deviation calculated from more than 10 independent measurements.

the photocurable hydrogel shell that mimics the extracellular connective tissue through the combination of an electrospinning and photo-cross-linking process (Figure 1). Poly(caprolactone) (PCL), silk fibroin (SF), and polyaniline (PANI) were blended together to prepare the aligned NFYs by a developed dry–wet electrospinning method. The poly(ethylene glycol)-*co*-poly(glycerol sebacate) (PEGS-M) polymer, a good biocompatible photocurable hydrogel material that has been studied in our previous work,[40] was chosen to prepare the hydrogel shell due to its ability to encapsulate cells for a long-term cultivation. Then, a series of core–shell column and sheet scaffolds were fabricated by encapsulating aligned NFY cores within the hydrogel shell after photo-cross-linking. The C2C12 myoblasts were seeded within these core–shell scaffolds to investigate the 3D cellular alignment and elongation behaviors. Moreover, after cultivation for 7 days, the myogenic differentiation and aligned myotube formation within these core–shell scaffolds were also investigated. We expect that these core–shell scaffolds comprised the aligned NFY core that can guide the cellular alignment and elongated myotube formation, and the hydrogel shell that can provide a suitable 3D environment for nutrition exchange and mechanical protection will have a great potential for skeletal muscle tissue engineering applications.

RESULTS AND DISCUSSION

A schematic of the manufacturing process of aligned NFYs and the actual fabricated device are shown in Figure 2a,b. First, the PCL/SF/PANI solution was jetted out of the syringe in the presence of a high voltage to form the random nanofiber web on the surface of the water/ethanol solution, and then, this nanofiber web was drawn and lifted off the liquid surface by a rotating receptor to form the elongated nanofiber bundle. By continuously receiving random nanofibers on the liquid and at the same time collecting them with the winder, the continuous nanofiber yarns were obtained (Movie S1 in the Supporting Information). The dimension of the NFYs was adjusted by changing the drawing speed (the rotation rate of the receptor), as shown in Figure 2c–f. The diameter of the NFYs decreased from 165 ± 11 to 25 ± 4 μm by increasing the rotation rate of the receptor from 40 to 120 mm/min (Figure 2i). The mechanical properties of single NFYs were measured by a tensile test, and the results indicate that the force of single NFYs increased from 1.49 ± 0.05 to 4.02 ± 0.09 cN by increasing the diameter of NFYs from 25 ± 4 to 165 ± 11 μm (Figure S1 and Table S1 in the Supporting

Information). Furthermore, the strain of NFYs with different diameters ranged from 76 ± 5 to 107 ± 4%, which suggests that all of these NFYs show good elasticity. The microstructure of these NFYs was confirmed by scanning electron microscopy (SEM) observation. The SEM images in Figure 2g,h reveal that the well-defined yarns containing multiple continuous nanofibers organized with the same orientation were obtained, and the diameter of the nanofibers was controlled at the range of 600 to 900 nm when choosing the present electrospinning situation. In addition, the composition of these NFYs including PCL, SF, and PANI was successfully confirmed by energy dispersed spectroscopy (EDS) and Fourier transform infrared (FTIR) analysis (Figure S2 in the Supporting Information). We used the composite material containing PCL, SF, and PANI to prepare the electrospinning aligned nanofiber yarns because it is highly beneficial for muscle tissue engineering applications. PCL is a kind of widely used synthetic biomaterial for electrospinning due to its suitable mechanical properties, good biocompatibility, and controllable biodegradability and is approved by the FDA for clinical tissue engineering applications.[41] Moreover, some studies have demonstrated that blending a conducting polymer such as PANI into the electrospinning aligned fibers has a significant effect on the number and length of myotubes and their aligned morphologies, due to the synergistic effects of nanofiber alignment and electroactivity.[42−47] For instance, the aligned PCL/PANI nanofiber films prepared by electrospinning have been demonstrated in a previous report to have the ability to induce C2C12 cell alignment and differentiation in the 2D environment by synergistic effects of nanofiber alignment and electroactivity.[42] However, the hydrophobic property of PCL/PANI composite nanofibers would strictly limit the cell adhesion on the narrow 3D peripheral surface of aligned NFYs. Therefore, in this study, the silk fibroin, a hydrophilic natural elastic polymer, was chosen to blend into this electrospinning system to increase the bioactivity and hydrophilicity of aligned NFYs and then to improve the cell adhesion and proliferation ability on the narrow surface environment.[48] The composition of the aligned NFYs, however, is not limited to PCL, SF, and PANI, and other types of synthetic biomaterials that can easily be fabricated into nanofibers by electrospinning such as polylactide (PLLA) and poly(lactic-*co*-glycolic acid) (PLGA) and natural biomaterials such as chitosan can be used in this process. Moreover, these aligned NFYs can also be blended with other natural biopolymers such as collagen and gelatin to improve the cell adhesion and proliferation on the 3D surrounding surface.

To investigate the effect of the microstructure of an aligned nanofiber bundle on cell viability, alignment, and elongation behavior, C2C12 mouse myoblasts at a high density (1.0×10^6 cells/mL) were seeded and cultured on aligned NFYs with different diameters, including 50, 100, and 165 μm, and cells cultured on tissue culture polystyrene (TCP) as the 2D control group. After 3 days of cultivation, the live/dead fluorescent assay that stains living cells green and dead cells red was used to measure the cell viability, and the results are shown in Figure 3a. The data indicate that approximately 90% of the cells were alive during the 3 days of incubation, and there was no significant difference in cell viability observed when cells were cultured on aligned NFYs with different diameter (Figure 3a(i)). However, after being cultured for 3 days, C2C12 cells proliferated and completely filled the peripheral surface of aligned NFYs with diameters of 100 and 165 μm, while cells did not fully fill the aligned NFYs with a diameter of 50 μm, mainly because the aligned NFYs with a thinner diameter would limit cell adhesion on the narrower surface (Figure 3a(ii−iv)). Quantitative analysis of cellular elongation on aligned NFYs was measured by the cellular aspect ratio, which is defined as the ratio between the length of the longest line and the length of the shortest line across the nuclei (Figure 3b(i)). The statistical analysis shows that the cellular aspect ratios on aligned NFYs are significantly higher than that on the 2D TCP environment (Figure 3b(ii−vi)). Furthermore, the aspect ratios on aligned NFYs with diameter of 50 and 100 μm were as high as 9 ± 1.3 and 9 ± 1.4, while the aspect ratio decreased to 7 ± 0.5 when the diameter increased to 165 μm (Figure 3b(ii)). The fluorescence images also confirmed that cells on aligned NFYs with 50 and 100 μm diameters showed better elongation behavior than that with the 165 μm diameter, while cells showed normal morphologies on 2D TCP (Figure 3b(iii−vi)). These data demonstrated that decreasing the diameter of aligned NFYs significantly enhanced cell elongation behavior. Furthermore, the cell alignment behavior was estimated by the orientation of cells by measuring the angle between long axis of the cells and the direction of aligned NFYs, and the cells that angled within ±10° were considered to be aligned (Figure 3c(i)). Quantitative analysis of cell alignment results is shown in Figure 3c(ii−v), and these histograms of cellular alignment angles displaying the relative percentages of cells within ±10° increments demonstrated that most of cells on aligned NFYs were aligned, while cells on 2D TCP were random, and the relative alignment decreased with increasing diameter of the aligned NFYs. On aligned NFYs with diameters of 50 and 100 μm, roughly 95 and 97% of cells aligned within ±10° orientation, respectively, while increasing the diameter of the fiber to 165 μm decreased the cell alignment to 88% of cells. However, only about 13% of the cells aligned when cultured on 2D TCP. Therefore, these results indicate that the PCL/SF/PANI aligned NFYs have good biocompatibility and the ability to

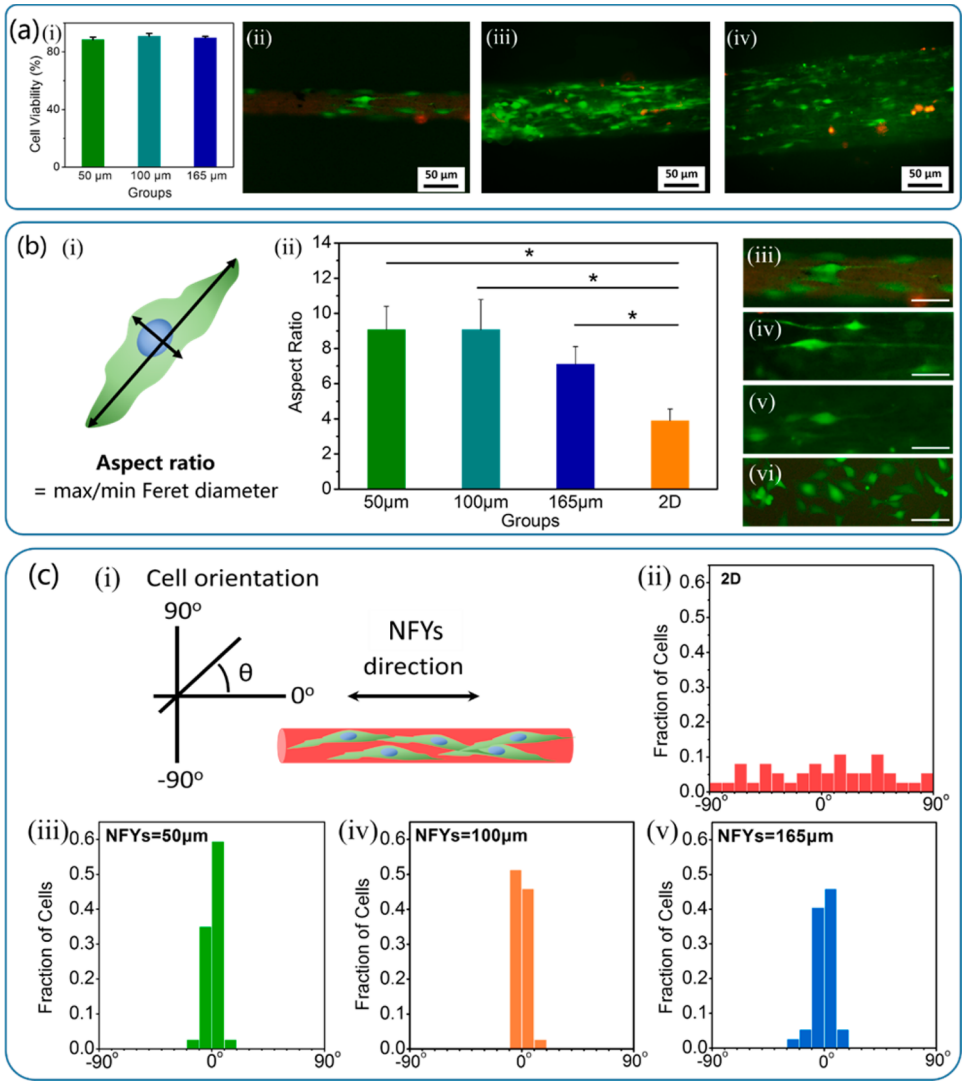

Figure 3. C2C12 cell viability, elongation, and alignment on aligned NFYs. (a) C2C12 cells were seeded on aligned NFYs with different diameters including 50, 100, and 165 μm and cultivation of 3 days, and then relative cell viability percentages were investigated (i). Live/dead fluorescent viability assay stained living cells green and dead cells red (ii−iv). (b) Cell elongation behavior was measured by aspect ratio (max/min Feret diameter) (i); the statistical analysis shows that the cellular aspect ratios significantly decreased with the increase of diameter, and cell cultivation on a 2D tissue culture of TCP served as the control group (ii). Fluorescent images of cellular elongation on aligned NFYs with different diameters (iii−v), where cells show normal morphologies on 2D TCP (vi). Scale bars = 30 μm. (c) Cell alignment behavior was estimated by the orientation of cells by measuring the angle between the long axis of the cells and the direction of aligned NFYs (i), and the histograms of the relative alignment in $\pm$10° increments demonstrate cellular alignment on aligned NFYs, in contrast to the random morphologies on 2D TCP (ii−v).

guide C2C12 cell elongation and alignment on their peripheral surface.

Although the aligned NFYs show the ability to induce cell elongation and alignment on their peripheral surface, the thin dimension and flexible mechanical properties of these aligned NFYs easily make them wind and twine together disorderly when used in the complex practical environment; furthermore, the cells would be damaged or removed from their surface. Therefore, embedding aligned NFYs within the hydrogel shell not only can prevent the random winding and twinning of aligned NFYs and maintain the original nanofiber yarns' microstructure but also can protect the cell proliferation and arrangement within the 3D environment. Furthermore, some reports have shown that myotubes would differentiate to a more physiological striated state when cultured on substrates with muscle-tissue-like stiffness (~10 kPa),[49,50] which suggests that the hydrogel shell with similar stiffness of normal muscle tissues that mimicked a native extracellular matrix (ECM) would provide a much more suitable 3D microenvironment for myogenic differentiation and *in vivo* muscle tissue regeneration applications. Therefore, aligned NFY/hydrogel core−shell scaffolds that not only induce 3D myoblast alignment and elongation but also provide a suitable microenvironment for cellular nutrition exchange and mechanical protection would have

potential for skeletal muscle tissue engineering applications.

To test the operability and practicability of core–shell scaffolds, the core–shell column scaffolds were first fabricated. The overall procedure to prepare core–shell column scaffolds is described in Figure 1. A piece of aligned NFYs was straightened and fixed within a frame mold and then placed into a poly(dimethylsiloxane) (PDMS) microtube pattern to act as the core. The PEGS-M, a good biocompatibility hydrogel material that has been researched in our previous study,[40] was added into the PDMS pattern and then formed the shell structure by photopolymerization under UV irradiation. In this study, we chose the PEGS-5M polymer (the methacrylation degree was 50%) to fabricate the hydrogel shell because its stiffness (11 $\pm$ 3 kPa) is in the same range of elasticity as normal muscle tissues ($\sim$10 kPa),[51,52] which would be beneficial for myogenic differentiation when C2C12 cells are cultured on the NFY core within this hydrogel shell. In addition, the PEGS-5M hydrogel exhibits an equilibrated swelling ratio of about 10, and water content of about 97% after swelling, which suggests that this hydrogel can provide large enough space for nutrition exchange and cell proliferation and differentiation within the hydrogel shell. Therefore, a series of core–shell column scaffolds containing aligned NFYs with different dimensions were fabricated by placing the aligned NFYs with the diameter ranging from 25 to 165 μm into the PEGS-M hydrogel column with a diameter of 550 μm, as shown in Figure 4a. The optical images of these core–shell column scaffolds revealed the presence and localization of the aligned NFY core within the hydrogel column shell (Figure 4a(i–iv)). Furthermore, to label an individually aligned NFY core and hydrogel shell, the aligned NFY core was stained red by mixing the Nile red fluorescence dye with the PCL/SF/PANI electrospun solution before electrospinning (Figure 4a(v–viii)), while the hydrogel shell was stained green by adding Alexa Fluor 488 fluorescence dye into the PEGS-M polymer solution before photo-cross-linking (Figure 4a(ix–xii)). These fluorescent images clearly showed the individually aligned NFY core and the hydrogel shell and further confirmed that the aligned NFYs were localized within the hydrogel shell very well (Figure 4a(xiii–xvi)). On the other hand, the hydrophobic Nile red dye and the hydrophilic Alexa Fluor 488 dye can also be regarded as the hydrophobic drug model and hydrophilic drug model, respectively, which suggests that the aligned NFY core loaded with hydrophobic drugs and the hydrogel shell loaded with hydrophilic drugs show the potential for sustained drug release applications. In addition, using this method, the core–shell scaffolds show that the aligned NFY core within the different diameter hydrogel column could also be fabricated, as shown in Figure S3 in the Supporting Information.

Comparing cell alignment and elongation in a 2D environment, design, and fabrication of scaffolds that can induce the controlled aligned and elongated cellular organization in a 3D environment is still an ongoing challenge. We expect that this problem would be easily resolved by culturing cells within these core–shell scaffolds due to the positive effect of cellular alignment and elongation on the aligned NFY core and the 3D environment protection of the hydrogel shell. Similar to seeding cells on the surface of aligned NFYs, first, the C2C12 cells were seeded on the aligned NFY core and allowed to attach for 24 h, and then, the hydrogel column shell was coated after photo-cross-linking. The cell-laden core–shell column scaffold was cultured within growth medium for another 2 days (Figure 4b(i)). The cell viability, alignment, and elongation behaviors were also investigated using a live/dead fluorescent viability assay. As shown in the fluorescent image of Figure 4b(ii) and its higher magnification image (Figure S4 in the Supporting Information), there are many more green spots (living cells) than red spots (dead cells), and the living cells exhibit the aligned and elongated organization, demonstrating that most of cells were viable; cellular alignment and elongation behaviors were also performed within this core–shell column scaffold. The morphologies of cells attached on nanofiber yarn for 24 h and then cultured within the hydrogel shell for another 2 days were both analyzed by a live/dead fluorescent viability assay (Figure S5 in the Supporting Information). From these fluorescence images, it showed that a majority of cells were attached and elongated on nanofiber yarn after 24 h. Furthermore, after being cured with hydrogel and continuous culturing for another 2 days, the cells were further elongated within the hydrogel. In addition, the aspect ratio of C2C12 cells was 5.8 on the nanofiber yarn, and it increased to 8.5 after 2 days of culturing in the composite scaffolds, revealing the continuous elongation of cells during the cultivation. Furthermore, the cell-laden aligned NFYs still showed the original linear structure during the cultivation, which was contributed by the 3D protection of hydrogels. Therefore, these results suggest that the aligned NFYs within the hydrogel core–shell column scaffolds would be highly beneficial for 3D cell alignment and elongation applications.

To further mimic the 3D aligned structure of skeletal muscle tissue and to confirm the clinical applications, the design of core–shell scaffolds is not limited to induce cell alignment and elongation on a piece of aligned NFY core within the hydrogel shell, but multiple layers of cell alignment and elongation within a 3D environment can be achieved. Therefore, complex core–shell sheet scaffolds that locate one layer or two layers of multiply aligned NFY cores within the hydrogel shell were designed and fabricated. Similar to

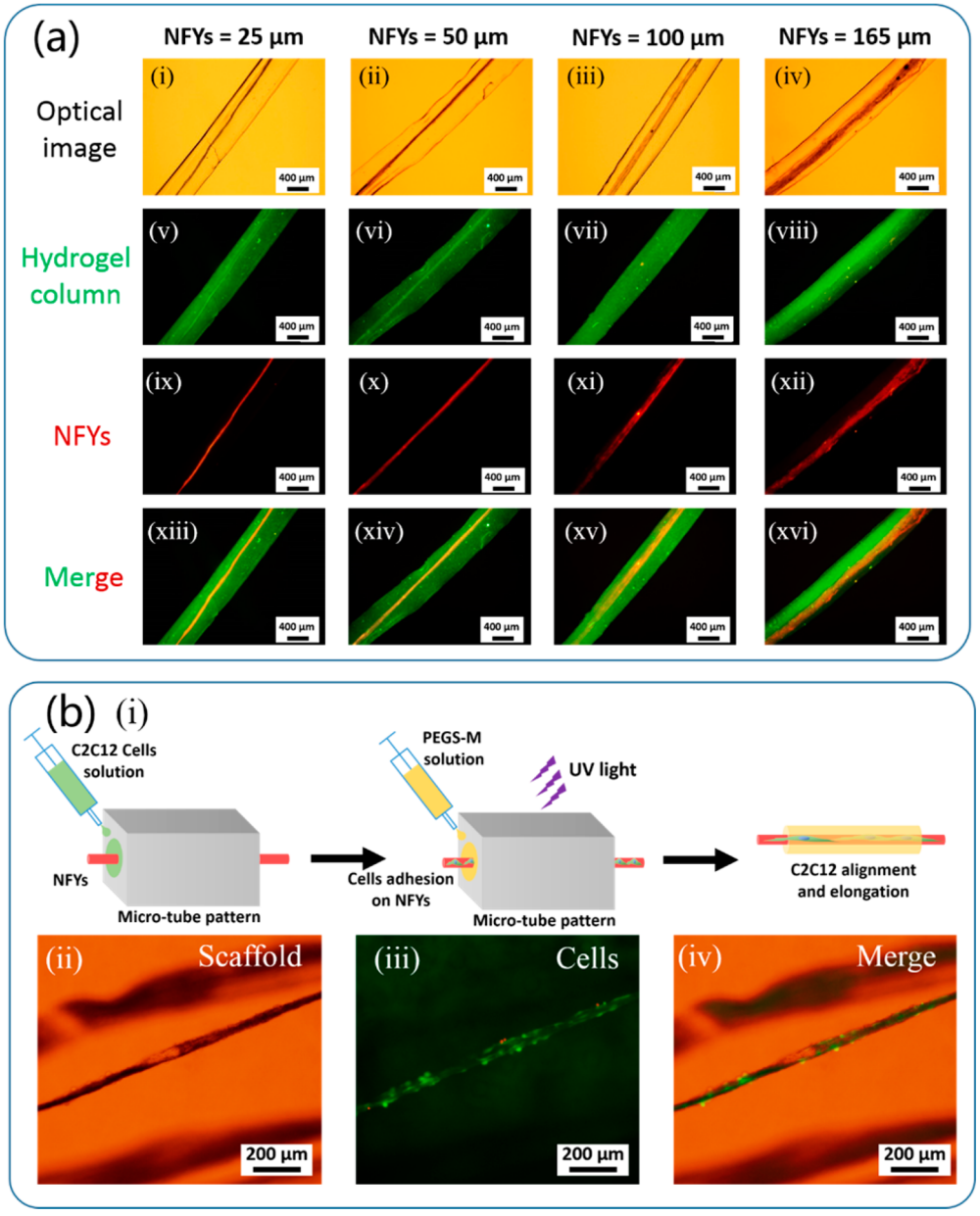

Figure 4. Fabrication of core–shell column scaffolds and cell cultivation within column scaffolds. (a) Optical microscopic images (i–iv) and fluorescent images (ix–xii) of an aligned NFY core with different diameters within the hydrogel column shell, green fluorescent images of hydrogel column shell (d = 550 μm) with Alexa Fluor 488 (v–viii), and red fluorescent images of aligned NFYs (d = 25–165 μm) with Nile red (ix–xii). (b) Scheme of C2C12 cells seeded and cultured within scaffolds (i). Optical microscopic image (ii), fluorescent image (iii), and merged image (iv) of C2C12 adhesion and proliferation on the aligned NFY core within the hydrogel column shell.

the procedure of core–shell column scaffold fabrication, the schematic process of core–shell sheet scaffold fabrication is shown in Figure 1. For the fabrication of core–shell sheet scaffolds with one layer of parallel aligned NFYs, a couple of aligned NFYs were straightened and fixed in a frame mold with the same orientation and then placed into a microsheet PDMS pattern to act as the one layer core. The PEGS-M polymer solution was added into the PDMS pattern, and then the hydrogel shell with a thickness of 1 mm was formed after photo-cross-linking (Figure 5a(i)). The optical images and fluorescent merged images revealed that a couple of parallel aligned NFYs with the same orientation were located well within the hydrogel sheet (Figure 5a(ii–iv)), and the higher magnification fluorescent merged images also exhibited an aligned nanofiber microstructure (Figure S6 in the Supporting Information). From the SEM images of core–shell sheet scaffolds after lyophilization (Figure S7 in the Supporting Information), both the nanofibrous structure of NFY cores and multiporous microstructure of the hydrogel shell were clearly observed from the cross section and the vertical section, and the NFY cores were placed within the hydrogel shell very well. In addition, the

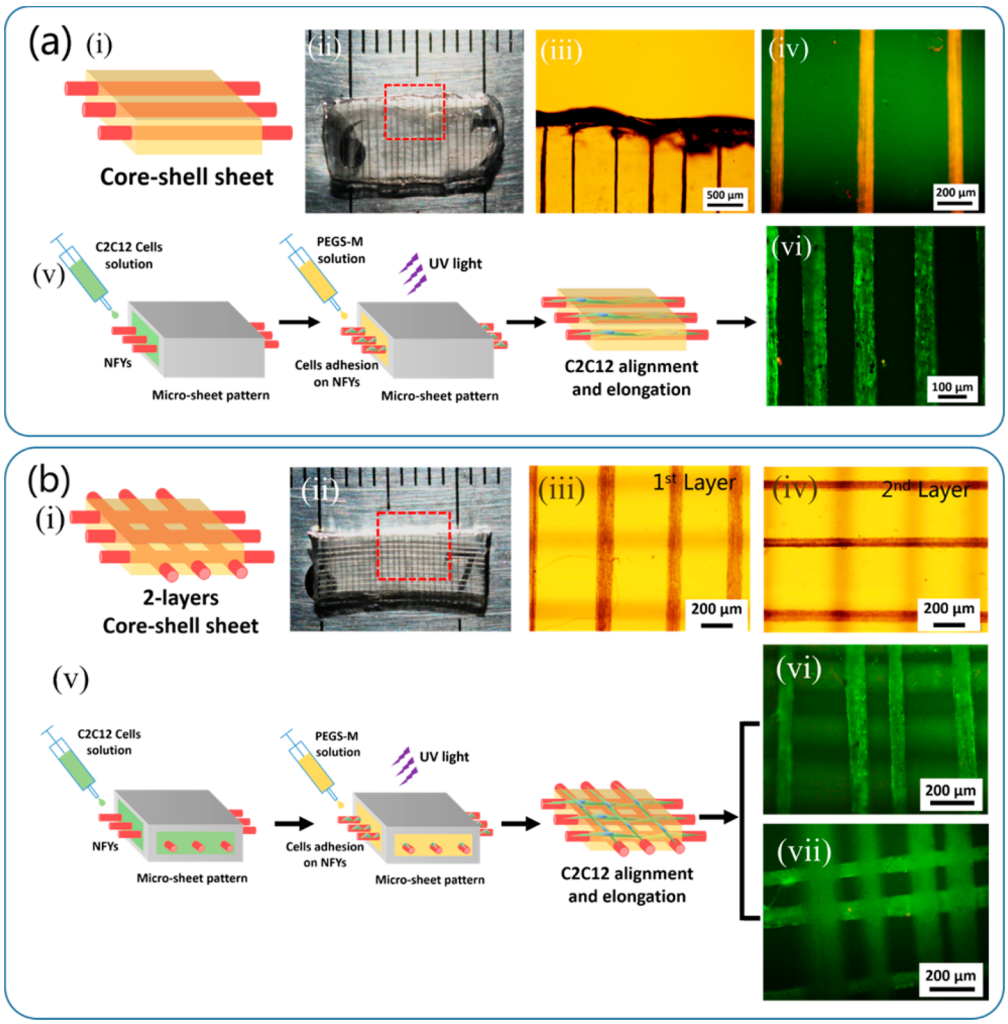

Figure 5. Fabrication of core–shell sheet scaffolds and cell cultivation within sheet scaffolds. (a) Scheme (i), optical images (ii,iii), and fluorescent merged image (iv) of core–shell sheet scaffolds containing one layer of parallel aligned NFYs within the hydrogel sheet. Scheme of C2C12 cells seeded and cultured within one-layer core–shell sheet scaffolds (v) and fluorescent merged image (vi) of aligned and elongated C2C12 cells fully filled on the aligned NFY core within the 3D hydrogel shell. (b) Scheme (i) and optical images (ii–iv) of two-layer core–shell sheet scaffolds containing two orthogonal layers of parallel aligned NFYs within the hydrogel sheet. The first layer (iii) and the second layer (iv) of parallel aligned NFYs with the orthogonal orientation were distinguished. Scheme of C2C12 cells seeded and cultured within two-layer core–shell sheet scaffolds (v) and fluorescent merged image (vi,vii) of aligned and elongated C2C12 cells fully filled on two orthogonal layers of the aligned NFY core within the 3D hydrogel shell.

porosity of core–shell sheet scaffolds after lyophilization was as high as 86.2 ± 5.8%, which also confirmed the multiporous microstructure of these scaffolds (Figure S8 in the Supporting Information).

The C2C12 cells were further seeded and cultured on these parallel aligned NFYs within the hydrogel sheet by using the same procedure of cultivation cells within core–shell column scaffolds (Figure 5a(v)). From the fluorescence image, it shows that the cells proliferated and were fully filled on the peripheral surface of these parallel aligned NFYs, and the cell alignment and elongation morphologies were both observed within the core–shell sheet scaffold (Figure 5a(vi)). The long-term cell viability within this core–shell scaffold at day 1, day 4, and day 7 was investigated by using the Alamar Blue method (Figure S9 in the Supporting Information). After being cultured for 4 days, cells maintained viability and proliferation on the aligned NFY core within the hydrogel shell compared to that on the first day. From day 4 to day 7, C2C12 cell proliferation slightly increased during the last 3 days of culturing, which may be due to the differentiation of cells. These results demonstrated the good long-term viability of C2C12 myoblasts in the core–shell composite scaffolds. In order to prove the ability to guide multiple layers of cellular alignment and elongation within a 3D environment by using this core–shell fabrication technique, we designed and fabricated the two-layer core–shell sheet scaffolds using the same process as use for fabrication of the one-layer core–shell sheet scaffold (Figure 1 and Figure 5b(i)). There are two layers of parallel aligned NFYs with orthogonal orientation to be encapsulated into the hydrogel sheet, as observed in the optical images and fluorescence merge images

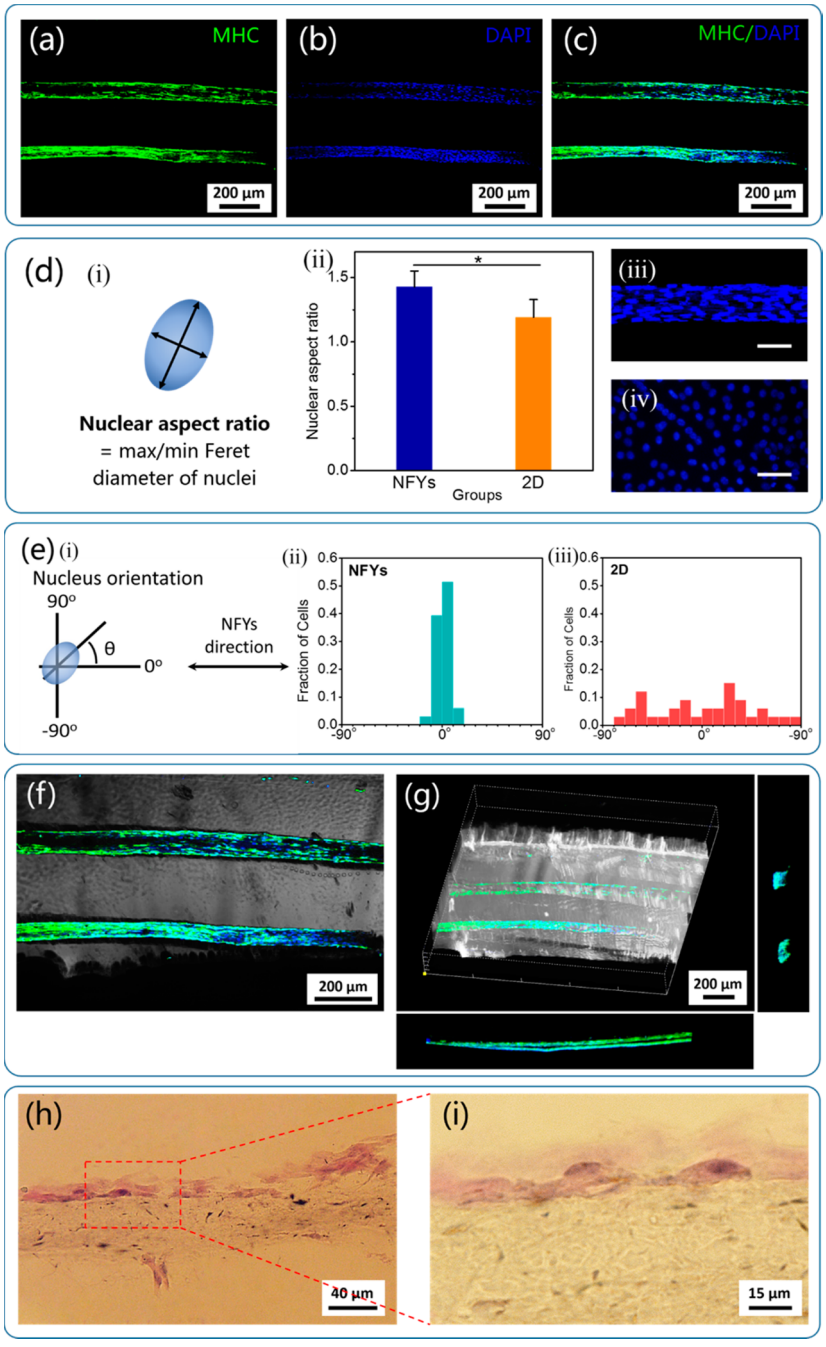

Figure 6. C2C12 cell myogenic differentiation within core–shell sheet scaffolds. Immunofluorescent images of myosin heavy chains (stained with green) (a), nucleus (stained with blue) (b) for C2C12 cells within core–shell sheet scaffolds, and the merged image (c) of MHC and nucleus. (d) Nuclear aspect ratio was defined as the max/min Feret diameter of cell nuclei (i), and the statistical analysis shows that the nuclear aspect ratios of cells within sheet scaffolds are significantly higher than that on 2D TCP (ii). Fluorescent images of the cell nuclei within scaffolds (iii) and on TCP (iv). Scale bars = 50 μm. (e) Myotube alignment was estimated by the nuclear orientation of cells by measuring the angle between the long axis of the nuclei and the direction of aligned NFYs (i), and the histograms of the relative alignment in $\pm 10^{\circ}$ increments demonstrate that most of the myotubes were aligned within the scaffolds and were random on 2D TCP (ii,iii). (f) Merged image of aligned NFY cores showing the overspreading of C2C12 myotubes within the hydrogel sheet. (g) Three-dimensional side view of the core–shell scaffolds containing highly organized synthetic myotubes. H&E staining image (h) and its higher magnification image (i) of C2C12 cells after cultivation for 7 days within core–shell scaffolds.

(Figure 5b(ii) and Figure S10 in the Supporting Information). Furthermore, as shown in the optical images with different focus distance, the two layers of parallel aligned NFYs with orthogonal orientation were distinguished very clearly (Figure 5b(iii,iv)). Analogously, after 3 days of cell cultivation within these two-layer core–shell sheet scaffolds, the aligned and elongated C2C12 cells were fully filled on the two layers of these parallel aligned NFYs within the 3D hydrogel sheet. These promising results demonstrate

that using this core−shell fabrication technique can easily develop the more complex core−shell scaffolds containing one layer, two layers, or even multiple layers of aligned NFY cores within a 3D hydrogel sheet, exhibiting the ability to control multiple layers of cellular alignment and elongation within a 3D environment and further suggesting the great potential applications for skeletal muscle tissue engineering.

Since aligned and elongated myotube formation in a 3D environment is crucial for maximizing the simulation of skeletal muscle tissue's natural structure and its contractility, we also investigated myogenic differentiation within the core−shell sheet scaffolds. The C2C12 cells were seeded on aligned NFY cores, and then the cell-laden aligned NFY cores were encapsulated within the hydrogel sheet. After 7 days of cultivation in growth medium, myotube formation of C2C12 cells was confirmed by immunofluorescence staining of myosin heavy chain (MHC). The immunofluorescent images showed that aligned and elongated C2C12 myotubes were fully filled on the peripheral surface of aligned NFY cores within the hydrogel sheet (Figure 6a−c,f). These data indicated that the core−shell scaffolds have the ability to induce C2C12 cell myogenic differentiation, even culture in growth medium, due to the good biocompatibility of the scaffolds and the NFYs' aligned structure. Correspondingly, the nuclear aspect ratio and alignment behavior were measured using ImageJ software to quantitatively evaluate overall C2C12 myotube elongation and alignment (Figure 6d,e). Nuclei of cells within core−shell sheet scaffolds were found to have a significantly higher aspect ratio than that in the 2D TCP environment (Figure 6d(ii−iv)). In addition, more than 90% of myotubes aligned within ±10° of the preferred nuclear orientation in scaffolds (Figure 6e(ii)), while myotubes on 2D TCP showed no nuclear alignment preference (Figure 6e(iii)), which suggests that highly aligned and elongated myotubes were formed within the scaffolds. The existence of aligned and elongated C2C12 myotubes within the 3D hydrogel shell was further confirmed by the merged image in Figure 6g and Movie S2 in the Supporting Information, which shows the 3D side view of the core−shell scaffolds. In addition, as shown in Movie S3 in the Supporting Information, it also clearly revealed that aligned C2C12 myotubes were fully filled on the peripheral surfaces of the aligned NFY cores within the 3D hydrogel sheet, thus demonstrating that these core−shell scaffolds promoted the formation of highly organized synthetic myofibers within the 3D environment. On the other hand, H&E staining of the cell-laden core−shell scaffolds was performed by using cryosection, and the results showed that NFY cores were surrounded by organized, elongated cells within the hydrogel shell, and a myofiber-like structure was formed in parallel rows on the surface of the NFY cores (Figure 6h,i). Furthermore, in the peripheral of nanofiber yarn, abundant ECM stained with eosin can be observed (Figure S11 in the Supporting Information), which indicated that cells formed a skeletal-muscle-like matrix within these core−shell scaffolds.

CONCLUSIONS

In summary, we developed a simple technique to fabricate a series of core−shell scaffolds composed of an electrospinning aligned nanofiber yarn core and a photocurable hydrogel shell for mimicking the native skeletal muscle tissue. The NFYs were prepared by a developed dry−wet electrospinning method, and then a series of core−shell column and sheet scaffolds were fabricated by encapsulating aligned NFY cores within a hydrogel shell after photo-cross-linking. C2C12 myoblasts were seeded on the aligned NFYs, and cultivation results demonstrated the good biocompatibility of these aligned NFYs and their ability to induce cellular alignment and elongation. Furthermore, the cells were cultured within core−shell scaffolds, and the 3D cellular alignment and elongation were confirmed by the fluorescent staining of cell-laden scaffolds. We also investigated the myogenic differentiation within the sheet scaffolds and demonstrated that these core−shell scaffolds enabled us to induce the 3D aligned and elongated myotube formation. These results suggest that by combining the aligned NFY core that guides the cellular alignment and elongated myotube formation and the hydrogel shell that provides a suitable 3D environment for nutrition exchange and mechanical protection, these novel core−shell composite scaffolds perform a great practical application for skeletal muscle regeneration.

EXPERIMENTAL SECTION

Synthesis and Preparation of Polymers. Polyaniline in the emeraldine salt (ES) form [PANI(ES)] was synthesized according to a previously reported method.[53] In brief, aniline (0.30 g, 3.2 mmol) (Sigma-Aldrich) was dissolved in 0.1 mol/L HCl (J&K), and then ammonium persulfate (APS, J&K) (0.73 g, 3.2 mmol) in 0.1 mol/L HCl solution was then added drop by drop to the above solution during 30 min with magnetic stirring. The reaction was carried out in air for 4 h at room temperature. The resulting mixture was added into ethanol (30:70 v/v) (J&K) and then filtered to collect the PANI with ES form. The PANI with emeraldine base (EB) form was obtained by treating PANI (ES) with 0.1 mol/L NH_4OH (J&K) solution for 24 h. The resulting dark-blue solid was filtered and washed by distilled water until the filtrate became neutral. Finally, the PANI (EB) was dried under vacuum for 72 h. Degummed silk (Buke Pharmaceutical Co.) was dissolved in $CaCl_2/H_2O$/ethanol (J&K) ternary solution (molar ratio 1:8:2) at 70 °C for 6 h. After dialysis (M_w = 3500 Da) in distilled water for 3 days, the resulting solution was filtered and then lyophilized to obtain the regenerated silk fibroin sponges. The synthesis of the PEGS-M copolymer was carried out *via* two stages according to our previous report.[40] First, the PEGS polymer was synthesized

by the polycondensation of sebacic acid (SAA, Sigma-Aldrich), poly(ethylene glycol) (PEG, M_n = 6 kDa, Sigma-Aldrich), and glycerol (Sigma-Aldrich) at 130 °C under nitrogen atmosphere for 3 h and then under reduced pressure (5 kPa) for another 24 h. Second, the PEGS-M copolymer was obtain *via* the incorporation of 2-(methacryloyloxy)ethyl isocyanate (MOI, Sigma-Aldrich) and PEGS copolymer in anhydrous tetrahydrofuran (THF, Sigma-Aldrich) at 62 °C under nitrogen atmosphere for 12 h. The product was precipitated from THF in diethyl ether (J&K) and was then dried at room temperature for 48 h under reduced pressure.

Preparation of PCL/SF/PANI Aligned NFYs. The aligned PCL/SF/PANI nanofiber yarns were prepared by employing a developed dry−wet electrospinning process. PCL (M_n = 80 kDa, Sigma-Aldrich), SF, and PANI were blended and dissolved in hexafluoroisopropanol (HFIP, Sigma-Aldrich) at room temperature for 24 h, and then camphorsulfonic acid (CSA, Sigma-Aldrich) was added into this solution to dope with PANI. The final concentrations of each material is as follows: PCL 120 mg/mL, SF 30 mg/mL, PANI 1.5 mg/mL, CSA with the same concentration of PANI. The schematic diagram in Figure 2a illustrates the working principle of this electrospinning device. In brief, the PCL/SF/PANI solution was placed into a syringe with a 21 G needle, and the volume flow rate of 1 mL/h was maintained using a syringe pump (Longer PrecisionPump, Baoding, China). For electrospinning, a voltage of 12 kV was applied by using a high-voltage power supply (Dongwen High Voltage Power Supply Plant, Tianjin, China). The nanofibers initially forming a random web were first received on the distilled water/ethanol (8:2 v/v) surface, and then this random nanofiber web was drawn and lifted off with a rotating receptor to form the continuous nanofiber yarns. The distance between the needle and the liquid surface was about 15 cm, and the rotating rate of the receptor was applied at 40, 80, 100, and 120 mm/min. The electrospun NFYs were collected and characterized using an inverted microscope (IX53, Olympus). The microstructure surface chemistry of NFYs was analyzed by scanning electron microscopy (SU-8010, Hitachi) with EDS capability, and the composition of NFYs was measured by FTIR spectra (NICOLET 6700, Thermo). Mechanical testing of single NFYs was performed on an electronic strength tester for a single fiber (YG001A, Precision Instruments Co., Shanghai). Uniaxial tensile testing was carried out at a stretching rate of 30 mm/min until specimen failure ($n \geq 4$ per sample).

Fabrication of Aligned NFYs within Hydrogel Core−Shell Scaffolds. To fabricate the core−shell column scaffold, a single piece of aligned NFYs was straightened and fixed within a frame mold and then placed into the PDMS microtube (Sylagrad 184, Dow Corning) pattern (diameter of the microtube = 550, 650, and 950 μm), while multiple pieces of aligned NFYs with the same orientation were placed into the PDMS microsheet pattern (16 mm × 8 mm × 1 mm) to fabricate the core−shell sheet scaffold. In addition, for the two-layer core−shell sheet scaffold fabrication, there are two layers of multiple pieces of aligned NFYs with the orthogonal direction placed into the PDMS microsheet pattern (16 mm × 8 mm × 1 mm). The PEGS-M hydrogel shells were then prepared by UV irradiation. The PEGS-M polymer was dissolved in deionized water (25% w/v), and then the Irgacure 2959 (Sigma-Aldrich) as photoinitiator (0.05% w/v) was added into the PEGS-M solution to initiate photopolymerization. The PEGS-M solution was dropped into the micro-PDMS pattern that contained NFY cores and was subsequently photopolymerized at 365 nm UV light at ~12 mW/cm^2 for 30 s. In order to label individual NFY cores and hydrogel shells, Nile red (Sigma-Aldrich) was mixed with the PCL/SF/PANI electrospun solution before electrospinning and Alexa Fluor 488 (Sigma-Aldrich) was mixed with the PEGS-M polymer solution before photo-cross-linking. The core−shell scaffolds were removed from the PDMS pattern and then characterized using an inverted microscope (IX53, Olympus) and a fluorescence microscope (IX53, Olympus). The microstructure of core−shell scaffolds was observed with a SEM (SU-8010, Hitachi) after freeze-drying. The porosity of the hydrogel shell and core−shell scaffold was measured with the following method. After being freeze-dried, the scaffold was cut into a regular cuboid and weighed (W_g), and its geometric volume (V_g) was calculated. The dried scaffold was immersed in acetone solution until the weight equilibrium (W_e) was reached. The porosity (P) of the scaffold was calculated by

$$P = \frac{(W_e - W_g)\rho_a}{V_g} \times 100\%$$

where ρ_a is the density of acetone.

C2C12 Cell Culture. C2C12 mouse myoblasts were purchased from Shanghai Cell Bank of Chinese Academy of Sciences. C2C12 cells were cultured in Dulbecco's modified Eagle medium (DMEM, GIBCO) supplemented with 10% fetal bovine serum (FBS, GEMINI), 100 U/mL penicillin (GIBCO), and 100 U/mL streptomycin (GIBCO) in an incubator at 37 °C in 5% CO_2. When confluence reached 90%, C2C12 cells were passaged as 1:4 by digestion with 0.25% trypsin (GIBCO).

C2C12 Cell Cultivation on Aligned NFYs. C2C12 cells were seeded and cultured on the PCL/SF/PANI aligned NFYs as described in the following process. First, the aligned NFYs were fixed within the rectangular groove of the PDMS mold and then sterilized by UV light for 2 h. Before being seeded with C2C12 cells, sterile aligned NFYs were incubated with cell culture medium at 37 °C for 2 h. Then, 0.4 mL of cell suspension (1.0×10^6 cells/mL) was dropped onto the aligned NFYs within the PDMS mold and incubated for 4 h. After it was confirmed that C2C12 cells adhered onto nanofiber yarns, another 1.6 mL of cell culture medium was added and cultivation continued for 3 days. The medium was changed every 2 days.

C2C12 Cell Cultivation within Core−Shell Scaffolds. C2C12 cell cultivation within core−shell scaffolds was performed with a process similar to the cultivation on the aligned NFYs. In brief, C2C12 cells were seeded and cultured on aligned NFYs for 24 h as described in the previous process, and then the cell-laden aligned NFYs were coated with the PEGS-M hydrogel shell after photo-cross-linking. For localization with the hydrogel, the cell-laden aligned NFYs were washed with DPBS (Dulbecco's phosphate-buffered saline) two times and then transferred into another PDMS mold with a certain shape. PEGS-M solution (prepared by culture medium) was immediately added into the PDMS mold containing the cell-laden aligned NFYs and then photopolymerized by UV irradiation at 12 mW/cm^2 for 30 s. The cell-laden aligned NFYs localized within the PEGS-M hydrogel shell were then transferred into a 35 mm Petri dish, and cultivation continued for another 2 days. The medium was changed every 2 days.

C2C12 Cell Viability, Elongation, and Alignment on Aligned NFYs or within Core−Shell Scaffolds. In order to investigate the biocompatibility of the PCL/SF/PANI aligned NFYs and PEGS-M hydrogels, a live/dead viability kit (Molecular Probes) was used. Cells were washed with DPBS two times for 10 min to remove the cell culture medium and treated with ethidium homodimer-1 (0.5 μM) and calcein AM (0.25 μM) for 45 min. Green color resulted from staining with calcein AM, indicating living cells, while red color resulted from staining with ethidium homodimer-1, indicating dead cells. The cell-laden constructs were observed under an inverted fluorescence microscope (IX53, Olympus) and analyzed using the ImageJ software. The elongation of C2C12 cells on aligned NFYs was quantitatively measured by aspect ratio, which was defined as the ratio between the length of the longest line and the length of the shortest line across the nuclei. The orientation of cells was determined from live/dead images by measuring the angle between the long axis of the cells and the direction of aligned NFYs to generate alignment histograms.[17] In addition, cell cultivation in a 2D tissue culture of TCP was considered to be the control group.

Long-Term Cell Viability within Core−Shell Scaffolds. The long-term cell viability of cells on NFYs within the hydrogel was evaluated by the Alamar Blue method (Molecular Probes). At each time point of the assay, these constructs were incubated in medium containing 10% (v/v) Alamar Blue reagent at 37 °C in 5% CO_2 for 5 h, then 100 μL of solution from each sample was removed into a 96-well plate and read at 530/600 nm in a SpectraMax fluorescence microplate reader (Molecular Devices). Medium containing 10% (v/v) Alamar Blue reagent served as a blank.

Differentiation Study of C2C12 Cells on Aligned NFYs within Scaffolds. After C2C12 cells were cultured on aligned NFYs that were localized with hydrogel shells in growth medium for 7 days, the cell constructs were rinsed twice gently with DPBS and then fixed with 2.5% glutaraldehyde for 15 min at room temperature. The fixed cell constructs were rinsed twice gently with DPBS and then treated with 0.3% Triton X-100 for 30 min. After being blocked in 1% BSA in DPBS for 1.5 h, the cell constructs were incubated in rabbit anti-MHC (myosin heavy chain) antibody (Santa Cruz) at 4 °C overnight. After being washed with DPBS, Alexa Fluor 488 conjugated secondary antibody (Molecular Probes) was added and incubated for 1.5 h at room temperature. Cell nuclei were counterstained with DAPI before observation under a confocal laser microscope (FV1200, Olympus).

H&E Staining of Cell-Laden Scaffolds. After being cultured for 7 days on NFYs within the hydrogel shell, these constructs were removed from the culture medium, washed with PBS three times, and fixed with 4% paraformaldehyde for 1 h. A 30% sucrose solution was used as the infiltration solution. Constructs were attached to a freezing stage using an optimum cutting temperature (OCT) compound and cut into 20 μm sections. The sections were air-dried for several hours before H&E staining.

Statistics. Quantitative data of cell aspect ratio were obtained using ImageJ software, and the results are from five images of three independent replications of the samples. Statistical differences were obtained through analysis of variance with a subsequent Tukey HSD multiple comparison test. A significance level of 0.05 was applied to determine significant differences.

Conflict of Interest: The authors declare no competing financial interest.

Acknowledgment. The National Natural Science Foundation of China (Grant No. 21304073) and Xi'an Jiaotong University are acknowledged for financial support of this work.

Supporting Information Available: The Supporting Information is available free of charge on the ACS Publications website at DOI: 10.1021/acsnano.5b03644.

Mechanical properties, surface chemistry, and porosity of the scaffolds, optical microscopic images, cell elongation and long-term viability of C2C12 cells on the scaffolds, fluorescence composite images, SEM of the core/shell scaffolds and H&E staining image of C2C12 cells after cultivation within core−shell scaffolds (PDF)
Movie S1 (AVI)
Movie S2 (AVI)
Movie S3 (AVI)

REFERENCES AND NOTES

1. Relaix, F.; Zammit, P. S. Satellite Cells Are Essential for Skeletal Muscle Regeneration: The Cell on the Edge Returns Centre Stage. *Development* **2012**, *139*, 2845–2856.
2. Brack, A. S.; Rando, T. A. Tissue-Specific Stem Cells: Lessons from the Skeletal Muscle Satellite Cell. *Cell Stem Cell* **2012**, *10*, 504–514.
3. Corona, B. T.; Wu, X.; Ward, C. L.; McDaniel, J. S.; Rathbone, C. R.; Walters, T. J. The Promotion of a Functional Fibrosis in Skeletal Muscle with Volumetric Muscle Loss Injury Following the Transplantation of Muscle-Ecm. *Biomaterials* **2013**, *34*, 3324–3335.
4. Stern-Straeter, J.; Riedel, F.; Bran, G.; Hoermann, K.; Goessler, U. R. Advances in Skeletal Muscle Tissue Engineering. *In Vivo* **2007**, *21*, 435–444.
5. Thorrez, L.; Shansky, J.; Wang, L.; Fast, L.; VandenDriessche, T.; Chuah, M.; Mooney, D.; Vandenburgh, H. Growth, Differentiation, Transplantation and Survival of Human Skeletal Myofibers on Biodegradable Scaffolds. *Biomaterials* **2008**, *29*, 75–84.
6. Jana, S.; Cooper, A.; Zhang, M. Chitosan Scaffolds with Unidirectional Microtubular Pores for Large Skeletal Myotube Generation. *Adv. Healthcare Mater.* **2013**, *2*, 557–561.
7. Li, L.; Ge, J.; Wang, L.; Guo, B.; Ma, P. X. Electroactive Nanofibrous Biomimetic Scaffolds by Thermally Induced Phase Separation. *J. Mater. Chem. B* **2014**, *2*, 6119–6130.
8. Qazi, T. H.; Mooney, D. J.; Pumberger, M.; Geißler, S.; Duda, G. N. Biomaterials Based Strategies for Skeletal Muscle Tissue Engineering: Existing Technologies and Future Trends. *Biomaterials* **2015**, *53*, 502–521.
9. Kim, S. J.; Cho, H. R.; Cho, K. W.; Qiao, S.; Rhim, J. S.; Soh, M.; Kim, T.; Choi, M. K.; Choi, C.; Park, I.; et al. Multifunctional Cell-Culture Platform for Aligned Cell Sheet Monitoring, Transfer Printing, and Therapy. *ACS Nano* **2015**, *9*, 2677–2688.
10. Wakelam, M. J. The Fusion of Myoblasts. *Biochem. J.* **1985**, *228*, 1–12.
11. Wigmore, P.; Dunglison, G. The Generation of Fiber Diversity During Myogenesis. *Int. J. Dev. Biol.* **1998**, *42*, 117–125.
12. Ostrovidov, S.; Hosseini, V.; Ahadian, S.; Fujie, T.; Parthiban, S. P.; Ramalingam, M.; Bae, H.; Kaji, H.; Khademhosseini, A. Skeletal Muscle Tissue Engineering: Methods to Form Skeletal Myotubes and Their Applications. *Tissue Eng., Part B* **2014**, *20*, 403–436.
13. Li, Y.; Huang, G.; Zhang, X.; Wang, L.; Du, Y.; Lu, T. J.; Xu, F. Engineering Cell Alignment *in Vitro*. *Biotechnol. Adv.* **2014**, *32*, 347–365.
14. Hosseini, V.; Ahadian, S.; Ostrovidov, S.; Camci-Unal, G.; Chen, S.; Kaji, H.; Ramalingam, M.; Khademhosseini, A. Engineered Contractile Skeletal Muscle Tissue on a Microgrooved Methacrylated Gelatin Substrate. *Tissue Eng., Part A* **2012**, *18*, 2453–2465.
15. Fujie, T.; Ahadian, S.; Liu, H.; Chang, H.; Ostrovidov, S.; Wu, H.; Bae, H.; Nakajima, K.; Kaji, H.; Khademhosseini, A. Engineered Nanomembranes for Directing Cellular Organization toward Flexible Biodevices. *Nano Lett.* **2013**, *13*, 3185–3192.
16. Hwang, C.; Park, Y.; Park, J.; Lee, K.; Sun, K.; Khademhosseini, A.; Lee, S. Controlled Cellular Orientation on Plga Microfibers with Defined Diameters. *Biomed. Microdevices* **2009**, *11*, 739–746.
17. Jana, S.; Leung, M.; Chang, J.; Zhang, M. Effect of Nano- and Micro-Scale Topological Features on Alignment of Muscle Cells and Commitment of Myogenic Differentiation. *Biofabrication* **2014**, *6*, 035012–1−12.
18. Bucaro, M. A.; Vasquez, Y.; Hatton, B. D.; Aizenberg, J. Fine-Tuning the Degree of Stem Cell Polarization and Alignment on Ordered Arrays of High-Aspect-Ratio Nanopillars. *ACS Nano* **2012**, *6*, 6222–6230.
19. Zan, X.; Feng, S.; Balizan, E.; Lin, Y.; Wang, Q. Facile Method for Large Scale Alignment of One Dimensional Nanoparticles and Control over Myoblast Orientation and Differentiation. *ACS Nano* **2013**, *7*, 8385–8396.
20. Huang, N. F.; Patel, S.; Thakar, R. G.; Wu, J.; Hsiao, B. S.; Chu, B.; Lee, R. J.; Li, S. Myotube Assembly on Nanofibrous and Micropatterned Polymers. *Nano Lett.* **2006**, *6*, 537–542.
21. Choi, J. S.; Lee, S. J.; Christ, G. J.; Atala, A.; Yoo, J. J. The Influence of Electrospun Aligned Poly (Epsilon-Caprolactone)/Collagen Nanofiber Meshes on the Formation of Self-Aligned Skeletal Muscle Myotubes. *Biomaterials* **2008**, *29*, 2899–2906.
22. Dugan, J. M.; Collins, R. F.; Gough, J. E.; Eichhorn, S. J. Oriented Surfaces of Adsorbed Cellulose Nanowhiskers Promote Skeletal Muscle Myogenesis. *Acta Biomater.* **2013**, *9*, 4707–4715.
23. Aviss, K.; Gough, J.; Downes, S. Aligned Electrospun Polymer Fibres for Skeletal Muscle Regeneration. *Eur. Cell Mater.* **2010**, *19*, 193–204.
24. Ma, P. X.; Zhang, R. Y. Microtubular Architecture of Biodegradable Polymer Scaffolds. *J. Biomed. Mater. Res.* **2001**, *56*, 469–477.
25. Kroehne, V.; Heschel, I.; Schuegner, F.; Lasrich, D.; Bartsch, J. W.; Jockusch, H. Use of a Novel Collagen Matrix with Oriented Pore Structure for Muscle Cell Differentiation in Cell Culture and in Grafts. *J. Cell. Mol. Med.* **2008**, *12*, 1640–1648.
26. Yang, H. S.; Ieronimakis, N.; Tsui, J. H.; Kim, H. N.; Suh, K. Y.; Reyes, M.; Kim, D. H. Nanopatterned Muscle Cell Patches for Enhanced Myogenesis and Dystrophin Expression in a Mouse Model of Muscular Dystrophy. *Biomaterials* **2014**, *35*, 1478–1486.

27. Drury, J. L.; Mooney, D. J. Hydrogels for Tissue Engineering: Scaffold Design Variables and Applications. *Biomaterials* **2003**, *24*, 4337–4351.
28. Lee, K. Y.; Mooney, D. J. Hydrogels for Tissue Engineering. *Chem. Rev.* **2001**, *101*, 1869–1880.
29. Hoffman, A. S. Hydrogels for Biomedical Applications. *Adv. Drug Delivery Rev.* **2012**, *64*, 18–23.
30. Cheema, U.; Yang, S. Y.; Mudera, V.; Goldspink, G. G.; Brown, R. A. 3-D *in Vitro* Model of Early Skeletal Muscle Development. *Cell Motil. Cytoskeleton* **2003**, *54*, 226–236.
31. Rhim, C.; Lowell, D. A.; Reedy, M. C.; Slentz, D. H.; Zhang, S. J.; Kraus, W. E.; Truskey, G. A. Morphology and Ultrastructure of Differentiating Three-Dimensional Mammalian Skeletal Muscle in a Collagen Gel. *Muscle Nerve* **2007**, *36*, 71–80.
32. Smith, A. S. T.; Passey, S.; Greensmith, L.; Mudera, V.; Lewis, M. P. Characterization and Optimization of a Simple, Repeatable System for the Long Term *in Vitro* Culture of Aligned Myotubes in 3d. *J. Cell. Biochem.* **2012**, *113*, 1044–1053.
33. Bian, W.; Liau, B.; Badie, N.; Bursac, N. Mesoscopic Hydrogel Molding to Control the 3d Geometry of Bioartificial Muscle Tissues. *Nat. Protoc.* **2009**, *4*, 1522–1534.
34. Aubin, H.; Nichol, J. W.; Hutson, C. B.; Bae, H.; Sieminski, A. L.; Cropek, D. M.; Akhyari, P.; Khademhosseini, A. Directed 3d Cell Alignment and Elongation in Microengineered Hydrogels. *Biomaterials* **2010**, *31*, 6941–6951.
35. Hsieh, H.-Y.; Camci-Unal, G.; Huang, T.-W.; Liao, R.; Chen, T.-J.; Paul, A.; Tseng, F.-G.; Khademhosseini, A. Gradient Static-Strain Stimulation in a Microfluidic Chip for 3d Cellular Alignment. *Lab Chip* **2014**, *14*, 482–493.
36. Moutos, F. T.; Freed, L. E.; Guilak, F. A Biomimetic Three-Dimensional Woven Composite Scaffold for Functional Tissue Engineering of Cartilage. *Nat. Mater.* **2007**, *6*, 162–167.
37. Jang, J.; Oh, H.; Lee, J.; Song, T.-H.; Jeong, Y. H.; Cho, D.-W. A Cell-Laden Nanofiber/Hydrogel Composite Structure with Tough-Soft Mechanical Property. *Appl. Phys. Lett.* **2013**, *102*, 211914−1–211914−5.
38. Lee, H. J.; Park, Y. H.; Koh, W. Fabrication of Nanofiber Microarchitectures Localized within Hydrogel Microparticles and Their Application to Protein Delivery and Cell Encapsulation. *Adv. Funct. Mater.* **2013**, *23*, 591–597.
39. Akbari, M.; Tamayol, A.; Laforte, V.; Annabi, N.; Najafabadi, A. H.; Khademhosseini, A.; Juncker, D. Composite Living Fibers for Creating Tissue Constructs Using Textile Techniques. *Adv. Funct. Mater.* **2014**, *24*, 4060–4067.
40. Wu, Y.; Wang, L.; Guo, B.; Ma, P. X. Injectable Biodegradable Hydrogels and Microgels Based on Methacrylated Poly-(Ethylene Glycol)-Co-Poly(Glycerol Sebacate) Multi-Block Copolymers: Synthesis, Characterization, and Cell Encapsulation. *J. Mater. Chem. B* **2014**, *2*, 3674–3685.
41. Baji, A.; Mai, Y.-W.; Wong, S.-C.; Abtahi, M.; Chen, P. Electrospinning of Polymer Nanofibers: Effects on Oriented Morphology, Structures and Tensile Properties. *Compos. Sci. Technol.* **2010**, *70*, 703–718.
42. Ku, S. H.; Lee, S. H.; Park, C. B. Synergic Effects of Nanofiber Alignment and Electroactivity on Myoblast Differentiation. *Biomaterials* **2012**, *33*, 6098–6104.
43. Chen, M.-C.; Sun, Y.-C.; Chen, Y.-H. Electrically Conductive Nanofibers with Highly Oriented Structures and Their Potential Application in Skeletal Muscle Tissue Engineering. *Acta Biomater.* **2013**, *9*, 5562–5572.
44. Balint, R.; Cassidy, N. J.; Cartmell, S. H. Conductive Polymers: Towards a Smart Biomaterial for Tissue Engineering. *Acta Biomater.* **2014**, *10*, 2341–2353.
45. Jun, I.; Jeong, S.; Shin, H. The Stimulation of Myoblast Differentiation by Electrically Conductive Sub-Micron Fibers. *Biomaterials* **2009**, *30*, 2038–2047.
46. Guo, B.; Glavas, L.; Albertsson, A. C. Biodegradable and Electrically Conducting Polymers for Biomedical Applications. *Prog. Polym. Sci.* **2013**, *38*, 1263–1286.
47. Ma, X.; Ge, J.; Li, Y.; Guo, B.; Ma, P. X. Nanofibrous Electroactive Scaffolds from a Chitosan-Grafted-Aniline Tetramer by Electrospinning for Tissue Engineering. *RSC Adv.* **2014**, *4*, 13652–13661.
48. Lee, H.; Jang, C. H.; Kim, G. H. A Polycaprolactone/Silk-Fibroin Nanofibrous Composite Combined with Human Umbilical Cord Serum for Subacute Tympanic Membrane Perforation; an *in Vitro* and *in Vivo* Study. *J. Mater. Chem. B* **2014**, *2*, 2703–2713.
49. Engler, A. J.; Griffin, M. A.; Sen, S.; Bönnemann, C. G.; Sweeney, H. L.; Discher, D. E. Myotubes Differentiate Optimally on Substrates with Tissue-Like Stiffness Pathological Implications for Soft or Stiff Microenvironments. *J. Cell Biol.* **2004**, *166*, 877–887.
50. Griffin, M. A.; Sen, S.; Sweeney, H. L.; Discher, D. E. Adhesion-Contractile Balance in Myocyte Differentiation. *J. Cell Sci.* **2004**, *117*, 5855–5863.
51. Discher, D. E.; Janmey, P.; Wang, Y.-l. Tissue Cells Feel and Respond to the Stiffness of Their Substrate. *Science* **2005**, *310*, 1139–1143.
52. Discher, D. E.; Mooney, D. J.; Zandstra, P. W. Growth Factors, Matrices, and Forces Combine and Control Stem Cells. *Science* **2009**, *324*, 1673–1677.
53. Macdiarmid, A. G.; Epstein, A. J. Polyanilines - a Novel Class of Conducting Polymers. *Faraday Discuss. Chem. Soc.* **1989**, *88*, 317–332.